ACS APPLIED MATERIALS & INTERFACES

Research Article

www.acsami.org

Multifunctional Microstructured Polymer Films for Boosting Solar Power Generation of Silicon-Based Photovoltaic Modules

Jung Woo Leem, Minkyu Choi, and Jae Su Yu*

Department of Electronics and Radio Engineering, Kyung Hee University, 1732 Deogyeong-daero, Giheung-gu, Yongin-si, Gyeonggi-do 446-701, South Korea

Supporting Information

ABSTRACT: We propose two-dimensional periodic conical micrograting structured (MGS) polymer films as a multifunctional layer (i.e., light harvesting and self-cleaning) at the surface of outer polyethylene terephthalate (PET) cover-substrates for boosting the solar power generation in silicon (Si)-based photovoltaic (PV) modules. The surface of ultraviolet-curable NOA63 MGS polymer films fabricated by the soft imprint lithography exhibits a hydrophobic property with water contact angle of ~121° at no inclination and dynamic advancing/receding water contact angles of ~132°/111° at the inclination angle of 40°, respectively, which can remove dust particles or contaminants on the surface of PV modules in real outdoor environments (i.e., self-cleaning). The NOA63 MGS film coated on the bare PET leads to the reduction of reflection as well as the enhancement of both the total and diffuse transmissions at wavelengths of 300−1100 nm, indicating lower solar weighted reflectance (R_{SW}) of ~8.2%, higher solar weighted transmittance (T_{SW}) of ~93.1%, and considerably improved average haze ratio (H_{Avg}) of ~88.3% as compared to the bare PET (i.e., $R_{SW} \approx$ 13.5%, $T_{SW} \approx$ 86.9%, and $H_{Avg} \approx$ 9.1%), respectively. Additionally, it shows a relatively good durability at temperatures of ≤160 °C. The resulting Si PV module with the NOA63 MGS/PET has an enhanced power conversion efficiency (PCE) of 13.26% (cf., PCE = 12.55% for the reference PV module with the bare PET) due to the mainly improved short circuit current from 49.35 to 52.01 mA, exhibiting the PCE increment percentage of ~5.7%. For light incident angle-dependent PV module current−voltage characteristics, superior solar energy conversion properties are also obtained in a broad angle range of 10−80°.

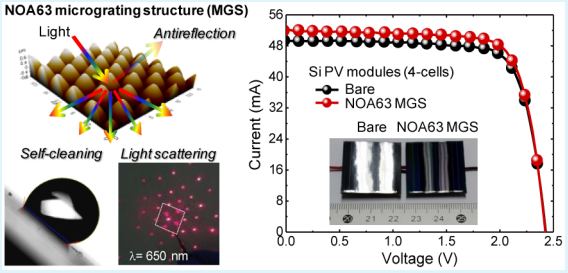

KEYWORDS: *micrograting structures, ultraviolet-curable polymer, silicon photovoltaic modules, soft imprint lithography, light harvesting, self-cleaning*

1. INTRODUCTION

Light harvesting in photovoltaic (PV) cells, which convert incoming solar photons to charge carriers, as an eco-friendly energy generation device has become crucial with the continuous improvement of cell design by coupling as much light as possible into the cell for effective enhancement of power conversion efficiency (PCE).[1−4] For this purpose, efficient broadband antireflection coatings (ARCs) are required on externally facing surfaces of PV cells to suppress Fresnel surface reflection losses. Most PV cells are packaged by cover-substrates (i.e., glasses, plastics, etc.) and adhesive glues for protection from exposure to external shock, heat, ultraviolet (UV) irradiation, and corrosive acidic rain in harsh outdoor environments.[5−7] In this respect, the ARCs should be also considered to reduce the reflection in PV module (panel) systems. However, conventional thin film ARCs using dielectric materials, which have some disadvantages such as poor or reduced substrate adhesion on certain materials, sensitivity to thickness variations, and material selection as well as narrow low reflection band for incident wavelengths and angles,[8,9] may not be suitable in practical harsh environments. As an alternative of conventional ARCs, over the past few years, there has been much research on the nano- or microtextured surfaces with efficient antireflection and light scattering properties for the PCE enhancement of PV cells or modules.[10−17] Particularly, bioinspired micrograting structures (MGS) with a tapered architecture can reduce the surface reflection in wide ranges of incident wavelengths and angles due to the formation of a gradient effective refractive index profile between air and the bulk surface, and thus the transmission can be enhanced for transparent substrates.[17−20] Besides, these microstructures can extend effective optical light-paths and promote diffuse lights in the absorption layer of PV modules, while keeping high total transmission (e.g., high haze).[17−20]

Soft imprint lithography has been widely employed to transfer nano- or micropatterns onto the UV-curable polymers from master molds using conformable and elastomeric poly dimethylsiloxane (PDMS) stamps, which have many advantages including low free surface energy, flexibility, transparency, and hardness because of its relative simplicity, low-cost, scale tunability, and high-throughput production[21,22] as compared to

Received: October 3, 2014
Accepted: January 15, 2015
Published: January 26, 2015

DOI: 10.1021/am5068194
ACS Appl. Mater. Interfaces 2015, 7, 2349−2358

the other expensive and complicated patterning methods such as electron beam (e-beam),[23] nanoimprint,[24,25] or photo[26,27] lithography, colloidal spheres,[28,29] metal nanoparticles,[30,31] etc., for etching mask patterns and subsequent dry etching processes. Also, once master molds and stamps are fabricated, they can be repeatedly used for pattern formations. Besides, the large-scale fabrication techniques of master molds and polymer stamps with nano- or micropatterns have been developed by roll-to-roll and roll-to-plate processes using the soft imprint lithography,[32,33] which would facilitate the mass-production of large-sized PV panels. However, to realize master molds with nano- or microarchitectures, in general, various patterning/dry etching processes are required.[23−31] Among these patterning methods, the photo lithography is a relatively simple, fast, cost-effective, easy-controllable, and large-scale technique without any post heat or chemical treatments as compared to e-beam or nanoimprint lithography, colloidal spheres, and thermally dewetted metal particles.[26,27]

Meanwhile, polyethylene terephthalate (PET) is widely used as device substrates and protective covers in rigid or flexible PV cell and module systems due to its good flexibility, lightweight, low-cost, and high-tolerance as well as good optical transparency.[33−36] At normal incidence, however, the reflectivity of ∼6% for a single-side surface of the PET with the refractive index (n) of ∼1.65 leads to the degradation of the optical performance in PV modules.[37] Recently, to enhance the light harvesting, many studies have been reported on antireflective structured polymers, for example, polycarbonate (PC),[19] PDMS,[22,38,39] poly(methyl methacrylate) (PMMA),[40,41] and polyurethane (PU),[42] with lower refractive indices than $n_{PET} \approx$ 1.65 for PV applications. However, these polymers are not appropriate in silicon (Si)-based PV systems, which absorb the sunlight at wavelengths of 300−1100 nm, because of their strong absorption at near-infrared (NIR) wavelengths of 800−1100 nm.[43−45] On the contrary, a UV-curable Norland Optical Adhesive (NOA) 63 polymer is very suitable as an ARC due to its lower refractive index of ∼1.56 as compared to the PET as well as almost no absorption in the wide wavelength region of 350−1100 nm.[46−48] In addition, the surface patterns are well formed using the soft lithography method because of its high Young's modulus (1655 MPa) including relatively good mechanical properties (i.e., hardness, robustness, and flexibility).[48−51] Furthermore, it is reported that there is no considerable discoloration or deterioration of the NOA polymer films coated on slide coverglasses, which were age-tested on UV exposure systems consisting of a rotating turntable and four 275 W-sunlamps positioned 10 in. away for 7 weeks and heat treatments in an oven at a temperature of 50 °C for 3 years.[46] In practice, however, because most of the PV modules are exposed to air with strong sunlight for a long time, a thermal durability of polymer films for protection should be also considered at high temperatures of >50 °C.

Hydrophobic property of textured surfaces is also useful to self-clean pollutants on the surface of PV modules in practical external applications.[52,53] The hydrophobic surface can be formed by the increased surface roughness, which can be explained by the Cassie and Baxter model, although it is also related to the surface energy of materials.[54−56] The highly transparent substrates with antireflective microstructures prepared by soft imprint lithography were reported in previous works,[19,42] but they just investigated their optical properties without any applications in PV cell or module systems. Thus, it is very meaningful to study the performance of PV modules incorporated with microstructured polymer films on the outer surface of PET cover-substrates including their surface wetting behaviors, thermal durability, and optical properties because there is very little or no report on the use of the conical MGS on the surface of polymer films as a light harvesting and protection layer of PET cover-substrates in PV modules using the soft imprint lithography.

In this Article, we demonstrated the boost of PCE in commercially available Si PV modules via the NOA63 MGS polymer films as the light harvesting and protection layer of PET cover-substrates. The MGS on NOA63 polymer films/PET substrates were transferred from conical MG patterned sapphire master molds via PDMS stamps by the soft imprint lithography technique. Their wettability, thermal durability, and optical characteristics were also investigated. The effect of the incident angle of light on the module performance was explored. For a theoretical analysis of optical light-propagation properties, the finite-difference time-domain (FDTD) simulation was also performed.

2. EXPERIMENTAL AND OPTICAL SIMULATION DETAILS

2.1. Fabrication and Characterization of NOA63 MGS Arrays.

Figure 1 shows the schematic illustration of the fabrication procedure

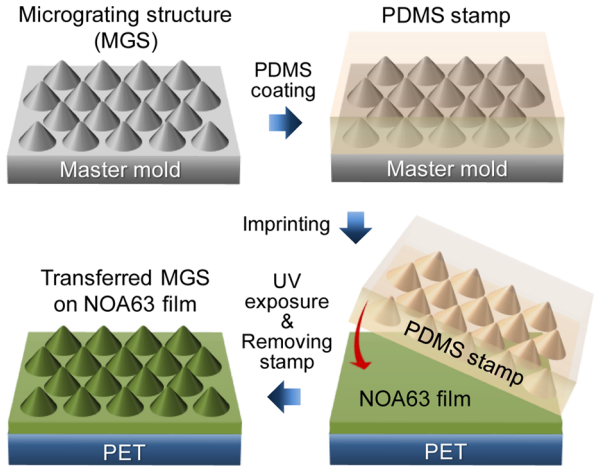

Figure 1. Schematic illustration of the fabrication procedure for conical MGS arrays on the surface of NOA63 polymer film/PET via a soft imprint lithography method.

for conical MGS arrays on the surface of NOA63 polymer film/PET via a soft imprint lithography method. To realize the MGS on the surface of NOA63 polymer films, two-dimensional (2D) periodic hexagonal tapered microcone array-patterned sapphire wafers (AND Corp.) with a diameter of 2 in., which were prepared by conventional photo lithography and subsequent inductively coupled plasma dry etching process with BCl_3/He mixture gases, were used as a master mold. It is noticeable that master molds can be also fabricated using various materials or substrates, besides the sapphire, by pattern formation methods such as e-beam,[23] imprint,[24,25] and photo[26,27] lithography techniques as well as colloidal spheres[28,29] and thermally dewetted metal particles,[30,31] etc. In this work, to effectively harvest the light in the absorption layer of Si PV modules, we chose tapered microgratings consisting of 2D periodic hexagonal pattern arrays with an average height of ∼1.5 μm and an average period of ∼2.9 μm. This structure had a strong diffuse light scattering in transmission, while keeping a high total transmission, over a wide wavelength range of 300−1100 nm.[17] The detailed optical properties can be found in our previous report.[17] As an imprint stamp, elastomeric PDMS templates

DOI: 10.1021/am5068194
ACS Appl. Mater. Interfaces 2015, 7, 2349−2358

were employed because of their good transparency as well as excellent formability for micropatterns. Commercial Sylgard 184 (Dow Corning Co.) mixed PDMS solution, consisting of a silicone "T-resin" cross-linked by a mixture of vinyl-terminated PDMS and trimethylsiloxyterminated poly(methylhydro-siloxane) polymers with a ratio of 10:1 (base:agent), was poured on master molds, and then cured at a temperature of 75 °C for 2 h. PDMS stamps were carefully separated from the master molds, which produces negative conical MG patterns. For the light harvesting and protection layer on the surface of PET cover-substrates, a UV-curable NOA63 (Norland Products Inc.) polymer solution was spin-coated on the PET at a rotation speed of 3000 rpm for 60 s and subsequently imprinted by PDMS stamps. The samples (PDMS stamp/NOA63 film/PET) were immediately exposed by UV radiation for 20 min, and the PDMS stamps were cautiously peeled off from the NOA63 film/PET, thus forming the NOA63 MGS/PET. The thickness of the remained NOA63 film was estimated to be ~10 μm. Similarly, to enhance the light harvesting in the underneath cell absorption layer of commercially available PV modules, the NOA63 MGS films were also prepared on PET cover-substrates of square-shaped crystalline Si PV modules with a total module active area of 7.29 cm^2 including metal contacts of cells, which were purchased from SolarCenter Co., Ltd., merged with four cells. The Si PV cells were completely encapsulated on a printed circuit board (PCB), together with an ethylene vinyl acetate (EVA) adhesive and a PET cover-substrate. The total thickness of encapsulants (i.e., EVA adhesive and PET cover-substrate) is approximately 1 mm. The surface morphologies and pattern/depth profiles of the MGS on the surface of NOA63 film/PET were characterized by using both scanning electron microscope (SEM; LEO SUPRA 55, Carl Zeiss) and atomic force microscope (AFM; XE150, psia) measurement systems. The optical transmittance and reflectance were investigated by using a UV−vis−NIR spectrophotometer (Cary 5000, Varian) with an integrating sphere at normal incidence. The water contact angles were measured and averaged at three different positions on the surface of samples by using a contact angle measurement system (Phoenix-300, SEO Co., Ltd.) with ~5 μL droplets of deionized water. The dynamic advancing and receding water contact angles were also explored on a precise control tilting stage with an inclination angle of 40°. A solar simulator (WXS-220S-L2, Wacom) was used for current−voltage measurements of PV modules under 1-sun air mass 1.5 global (AM1.5G, 100 mW/cm^2) illumination at room temperature.

2.2. Numerical Modeling and Simulation of NOA63 MGS Arrays. The theoretical analysis on optical light scattering behaviors of the tapered MG patterned NOA63 polymer film/PET was also carried out by the FDTD method. To design the theoretical model, in simulations, the conical MGS on NOA63 polymer films was represented by a periodic geometry in the Cartesian coordinate system by a scalar-valued function of two variables, $f(x, z)$, for simplicity. It was assumed that the incident light enters from air into the structure at normal incidence. The E_y, that is, amplitude of y-polarized electric field, was calculated for the incident plane wave with a Gaussian beam profile, which is normalized at a wavelength (λ) of 650 nm. The height and period of conical MGS on the NOA63 polymer film were kept at 1.4 and 2.9 μm, respectively. The thicknesses of NOA63 polymer film and PET were set to be 10 and 100 μm, respectively. The refractive index of the PET used in these calculations was acquired from the index Web site.[37] For the NOA63 polymer film, the refractive index was assumed to be 1.56, and the extinction coefficient was not considered because it can be negligible.[46−48]

3. RESULTS AND DISCUSSION

Figure 2 shows the 15 μm × 15 μm scan AFM images and depth profiles of the fabricated (a) PDMS stamp and (b) NOA63 MGS/PET. As shown in Figure 2a, it can be observed that the PDMS stamp, which was fabricated from the sapphire master mold, exhibits microscale grooved structures (i.e., negative conical MGS) with 2D periodic hexagonal array patterns. Using this PDMS stamp, the conical MGS was well

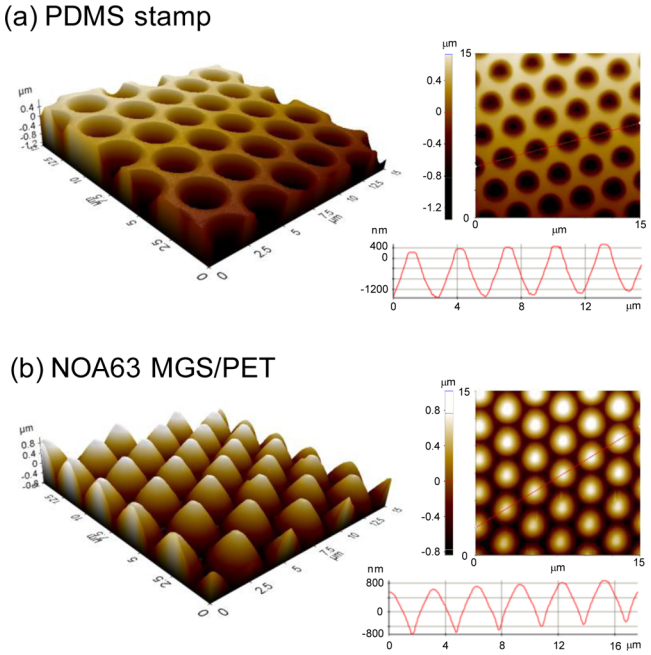

Figure 2. The 15 μm × 15 μm scan AFM images and depth profiles of the fabricated (a) PDMS stamp and (b) NOA63 MGS/PET.

transferred on the NOA63 polymer film/PET without any deformation and distortion, as can be seen in Figure 2b. For the formed NOA63 MGS, the average height and average period are approximately 1.4 and 2.9 μm, respectively. The ratio of the bottom diameter of MGS to the period between MGS is estimated to be ~0.9. Additionally, the SEM image in Figure S1(a) (Supporting Information) illustrates that the conical MGS on the NOA63 polymer film was very uniformly formed over a large area. From the photograph in Figure S1(b) (Supporting Information), the flexibility and robustness of NOA63 MGS polymer film coated on the PET (i.e., NOA63 MGS/PET) can be verified, and thus this architecture can be also used in various flexible device applications.

The dust particles or contaminants on the surface of protective covers in PV modules are very harmful to the module performance in external environments because they interfere with incident light into the cell absorption layer. Thus, it is necessary to fabricate the light harvesting and protection layer with a self-cleaning function for outdoor applications. Figure 3 shows the (a) photographs of a water droplet on the surface of the (i) bare PET and (ii) NOA63 MGS/PET at no inclination and (b) sequential photographs of water droplet cleaning behaviors for the corresponding samples. As shown in Figure 3a, the bare PET shows a hydrophilic surface with a water contact angle (θ_{CA}) of ~76°. On the contrary, the surface of the NOA63 MGS has a hydrophobic property, exhibiting the $\theta_{CA} \approx 121°$. This θ_{CA} value is much higher than that (i.e., $\theta_{CA} \approx 78°$) of the flat NOA63 film, as can be seen in Figure S2 (Supporting Information). The hydrophobic property of the NOA63 MGS film mainly originated from the enhanced surface roughness as proposed by the Cassie and Baxter model, although it is also related to the surface energy of materials.[54−56] Although this θ_{CA} value is relatively lower than those (i.e., $\theta_{CA} > 150°$, superhydrophobicity) reported in other works,[52,53] the dust particles on the hydrophobic surface with the $\theta_{CA} \approx 121°$ can be also washed by rainwater droplets because the NOA63 MGS polymer film has relatively large

DOI: 10.1021/am5068194
ACS Appl. Mater. Interfaces 2015, 7, 2349−2358

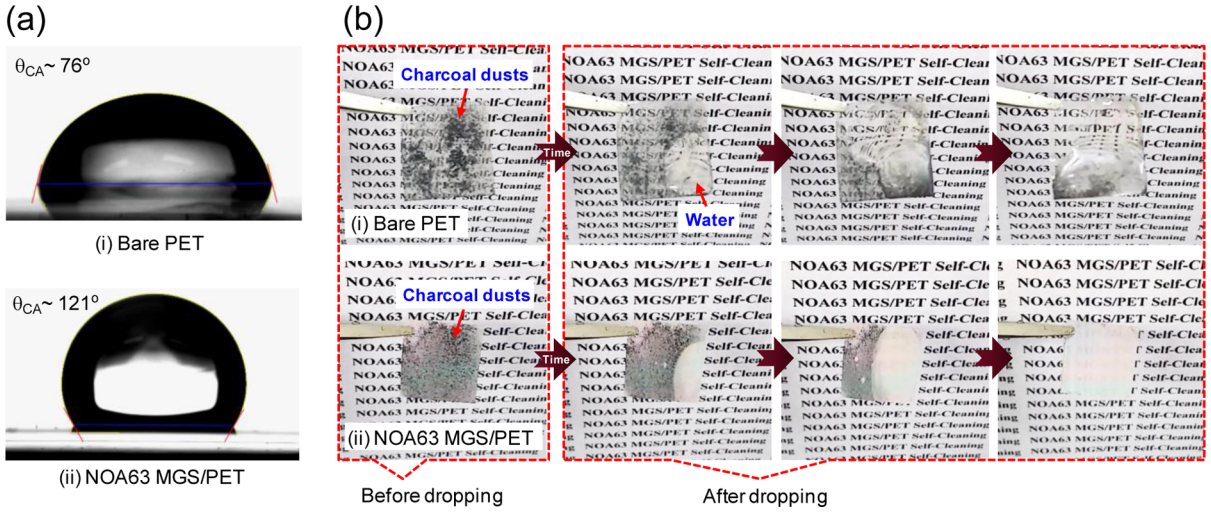

Figure 3. (a) Photographs of a water droplet on the surface of the (i) bare PET and (ii) NOA63 MGS/PET at no inclination and (b) sequential photographs of water droplet cleaning behaviors for the corresponding samples.

dynamic advancing (θ_{ACA}) and receding (θ_{RCA}) water contact angles of $\theta_{ACA} \approx 132°$ and $\theta_{RCA} \approx 111°$ at the inclination angle of 40°, respectively, exhibiting the contact angle hysteresis (i.e., $\theta_{ACA} - \theta_{RCA}$) of ~21° (see Figure S3 in the Supporting Information). As can be seen in Figure 3b, after dropping water droplets, the black charcoal dusts on the bare PET were just relocated by water droplets due to its hydrophilicity (i.e., $\theta_{CA} \approx 76°$), thus partially remaining with water droplets at its edge. For the NOA63 MGS/PET, in contrast, the black charcoal dusts were clearly removed by rolling-down water droplets without any remained droplets at the surface (i.e., self-cleaning). For this, the further detailed subdivided sequential photographs can be found in Figure S4 (Supporting Information). From these results, the NOA63 MGS polymer films with a hydrophobic surface can be very useful because the optical interface with an additional self-cleaning effect would enhance the practical feasibility in outdoor dusty environments.

Figure 4 shows the (a) measured total (specular + diffuse) transmittance and reflectance spectra, (b) spectral distributions of the photonic flux density (PFD) for the measured total transmittance spectra, and (c) measured diffuse transmittance spectra of the bare PET and NOA63 MGS/PET. For comparison, the optical properties of a flat NOA63 film/PET are shown in Figure S5 (Supporting Information). The NOA63 film without any patterns slightly increases the total transmission (or decreases the total reflection) of the bare PET at wavelengths of 300−1100 nm because of the gradient refractive index distribution in constituent materials of air (n = 1)/NOA63 (~1.56)/PET (~1.65), while there is almost no variation in the diffuse transmittance.[57−59] As can be seen in Figure 4a, on the other hand, the NOA63 MGS polymer film further enhances the total transmission (or suppresses the total reflection) of the bare PET over a broad wavelength range of 300−1100 nm. To investigate the influence of the transmission properties of NOA63 MGS/PET on the PV module performance, the solar photon flux-weighted transmittance (T_{SW}) was evaluated. The T_{SW} is defined by normalizing the transmittance spectra with the solar spectral photon flux (i.e., AM1.5G spectrum[60]) integrated over a wavelength range of 300−1100 nm.[61] The T_{SW} is given by

$$T_{SW} = \frac{\int F_{AM1.5G}(\lambda) T(\lambda)\, d\lambda}{\int F_{AM1.5G}(\lambda)\, d\lambda} \quad (1)$$

where $F_{AM1.5G}(\lambda)$ is a spectral irradiance and $T(\lambda)$ is the total transmittance in Figure 4a. For the NOA63 MGS/PET, the higher T_{SW} value of ~93.1% was obtained as compared to the bare PET (i.e., $T_{SW} \approx 86.9\%$). For the total reflectance, the solar photon flux-weighted reflectance (R_{SW}), which is similarly estimated from eq 1 by replacing the transmittance (T) with the reflectance (R), was also explored.[61] As expected, the R_{SW} value of the NOA63 MGS/PET was estimated to be ~8.2%, which is lower than that ($R_{SW} \approx 13.5\%$) of the bare PET. This is also ascribed to the conical MGS, which forms the linearly gradient effective refractive index profile from air to the NOA63 film and extends effective optical light-paths.[17−20,62] This low reflectivity can be also confirmed from the photograph of the inset of Figure 4a. The AR in the inset of Figure 4a is of the bare PET and NOA63 MGS/PET samples showing antireflection properties. For the bare PET, the characters underneath it are nearly not seen due to the strongly reflected white fluorescent light at the surface. However, the NOA63 MGS/PET exhibits a better legibility for the characters below the sample due to the weak reflected white fluorescent light although the characters are slightly blurred, which shows only modest effects of reflection for the NOA63 MGS/PET.

For the incident sunlight with different intensities at each wavelength, the transmission property can be also characterized by the calculation of the PFD, which is the number of solar photons transmitted across the transparent sample.[63,64] The PFD gives information that the PV cell could produce photocurrents at specific wavelengths of solar spectrum. The PFD is obtained by

$$\mathrm{PFD}(\nu) = \frac{F_{AM1.5G} T}{h\nu} \quad (2)$$

where $F_{AM1.5G}$ is a spectral irradiance, T is the total transmittance in Figure 4a, and $h\nu$ is a photon energy. In Figure 4b, the NOA63 MGS/PET exhibits a higher PFD spectral distribution over a wide wavelength region of 300−1100 nm as compared to the bare PET, particularly at wavelengths of 400−600 nm, which are a high intensity range

DOI: 10.1021/am5068194
ACS Appl. Mater. Interfaces 2015, 7, 2349−2358

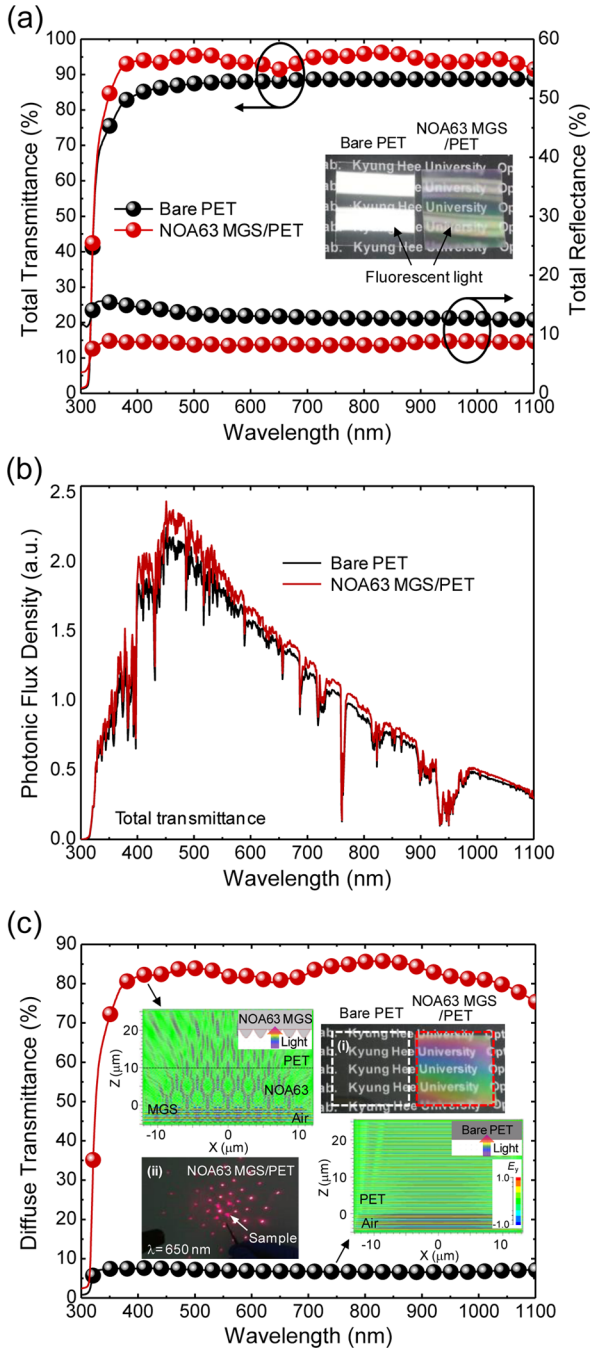

Figure 4. (a) Measured total transmittance and reflectance spectra, (b) spectral distributions of the PFD for the measured total transmittance spectra, and (c) measured diffuse transmittance spectra of the bare PET and NOA63 MGS/PET. Photograph of the bare PET and NOA63 MGS/PET samples for AR properties is shown in the inset of (a). Photographs of the (i) bare PET (white-dotted line) and NOA63 MGS/PET (red-dotted line) samples for the verification of light scattering properties and the (ii) diffraction phenomenon of the NOA63 MGS/PET using a laser with λ = 650 nm are shown in the insets of (c), respectively. Contour plots of E_y distributions for the incident light propagating from air to the bare PET and the NOA63 MGS/PET at λ = 650 nm including the corresponding scale-modified simulation models used in these calculations are also shown in the insets of (c).

in the AM1.5G solar spectrum. Therefore, it can be expected that larger photogenerated currents could be obtained from the cell absorption layer of PV modules incorporated with the NOA63 MGS/PET as compared to ones with the bare PET, and thus it leads to the efficiency enhancement of Si PV modules.[63,64]

For a periodic grating structure, when a light enters into the grating with a period of Λ at normal incidence, the angle of the transmitted diffraction waves, $\theta_{t,m}$, in the mth diffraction order is given by the well-known grating equation:[65]

$$\sin \theta_{t,m} = \frac{m\lambda}{\Lambda n} \tag{3}$$

where λ is the incident wavelength of light and n is the refractive index of the incident medium. For the transparent materials with low refractive indices including glasses, plastics, and sapphires, etc., the tapered structures with desirable microscale periods can lead to the enhancement of total and diffuse transmittances, simultaneously.[17−20] Therefore, similarly, the conical MGS polymer film also can increase both the total and the diffuse transmittances of the bare PET. As shown in Figure 4c, the NOA63 MGS/PET shows a much higher diffuse transmittance spectrum at wavelengths of 300−1100 nm, while there exist almost no diffracted lights for the bare PET. The haze ratio (H), which is given by the ratio of the diffuse transmission (T_d) to the total transmission (T_t), that is, $H(\%) = T_d/T_t \times 100$, is often used to investigate the light scattering property of a sample. For the NOA63 MGS/PET, a much larger average H (H_{Avg}) value of ~88.3% was achieved as compared to that ($H_{Avg} \approx 9.1\%$) of the bare PET at wavelengths of 300−1100 nm. In both the transmission and the reflection properties, high diffraction behaviors (i.e., light scattering) of the NOA63 MGS/PET can be observed in the insets of Figure 4c. Photographs in the insets of Figure 4c show the (i) bare PET (white-dotted line) and NOA63 MGS/PET (red-dotted line) samples for the verification of light scattering properties and the (ii) diffraction phenomenon of NOA63 MGS/PET using a laser with λ = 650 nm, respectively. In Figure 4c(i), as compared to the bare PET, the obvious light scattering phenomenon (i.e., rainbow colors) at the surface of the NOA63 MGS/PET sample is observed with the naked eye. It also shows higher order diffraction patterns in transmitted lights for λ = 650 nm in Figure 4c(ii). The contour plots of calculated electric field (E_y) distributions for the incident light propagating from air to the bare PET and the NOA63 MGS/PET at λ = 650 nm including the corresponding scale-modified simulation models used in these calculations are also shown in the insets of Figure 4c. From the FDTD simulation results, the NOA63 MGS with a period of 2.9 μm has a strong light scattering property with a wide angular spread and helps the light propagation across the interface between air and the NOA63 polymer film/PET, while there are no diffraction lights for the bare PET without any patterns.[17,20] It is noted that the NOA63 MGS polymer film enables one to increase the diffuse transmittance of the PET, while maintaining high total transmission, which can lead to the PCE improvement of PV modules due to the enhanced light harvesting (i.e., AR and light scattering properties) in the absorption layer of encapsulated PV devices.

Because most PV modules are exposed to air with strong sunlight for a long time, the thermal durability of polymers as a protection film should be considered. Thus, the effect of temperature on transmittance properties of NOA63 MGS polymer films was investigated. For this, the samples were heated in an oven for 10 h over a temperature range of 25−200

DOI: 10.1021/am5068194
ACS Appl. Mater. Interfaces 2015, 7, 2349−2358

°C. Figure 5 shows the T_{SW} value of the bare PET and NOA63 MGS/PET as a function of temperature in the wavelength

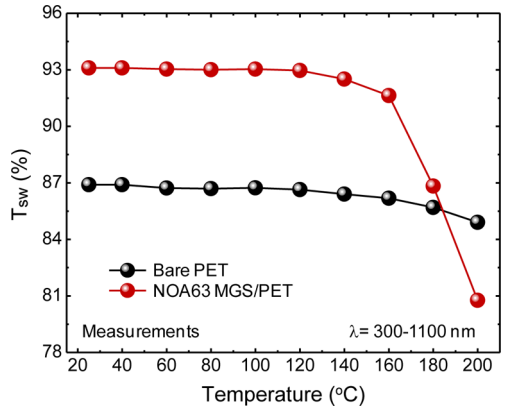

Figure 5. T_{SW} value of the bare PET and NOA63 MGS/PET as a function of temperature at λ = 300−1100 nm.

range of 300−1100 nm. For both the bare PET and the NOA63 MGS/PET, their transmission properties depend on the temperature. There is no significant variation in T_{SW} values up to a temperature of 160 °C, while maintaining T_{SW} values of ≥86.2% for the bare PET and ≥91.6% for the NOA63 MGS/PET, respectively. At temperatures of >160 °C, however, the T_{SW} value of the NOA63 MGS/PET is abruptly reduced by ~80.8% at 200 °C, while it is slightly decreased for the bare PET (i.e., $T_{SW} \approx$ 84.9% at 200 °C). This considerable degradation in the transmission is attributed to the distortion and deformation of the NOA63 MGS as well as the bowing of samples due to the thermal expansion mismatch between the NOA63 polymer and the PET caused by the long exposure time under high temperatures. Nevertheless, the T_{SW} value of ~91.6% at the high temperature of 160 °C is much larger than that (i.e., $T_{SW} \approx$ 86.9%) of the bare PET without heat treatments. As a result, it is noted that the NOA63 MGS polymer films have a relatively good durability at temperatures of ≤160 °C, which can show a feasibility in practical PV module systems.

To demonstrate the applicability of NOA63 MGS polymer films with efficient AR and light scattering effects in PV modules covered by a PET protection film, the reflection and device characteristics of PET laminated Si PV modules employed with the NOA63 MGS were investigated. Figure 6a and b shows the measured total reflectance spectra and current−voltage (I−V) characteristics of Si PV modules (four cells) with the bare PET and NOA63 MGS/PET at normal incidence, respectively. The schematic of the Si PV module with the NOA63 MGS/PET is also shown in the inset of Figure 6b. In Figure 6a, the reflectance spectrum of the Si PV module with the NOA63 MGS/PET is lower than that of the reference Si PV module with the bare PET over a wide wavelength range of 300−1100 nm, exhibiting the lower $R_{SW} \approx$ 6.3% (i.e., $R_{SW} \approx$ 11.2% for the reference Si PV module). This is attributed to the efficient AR characteristics caused by the formation of gradient effective refractive index profiles in the structure between air and the NOA63 film via the MGS and the constituent materials of air (n = 1)/NOA63 (~1.56)/PET (~1.65) as well as the extended effective optical light-paths by the MGS, as mentioned above.[17−20,57−59,62] This AR property can be also confirmed in the photograph of the inset of Figure 6a, which

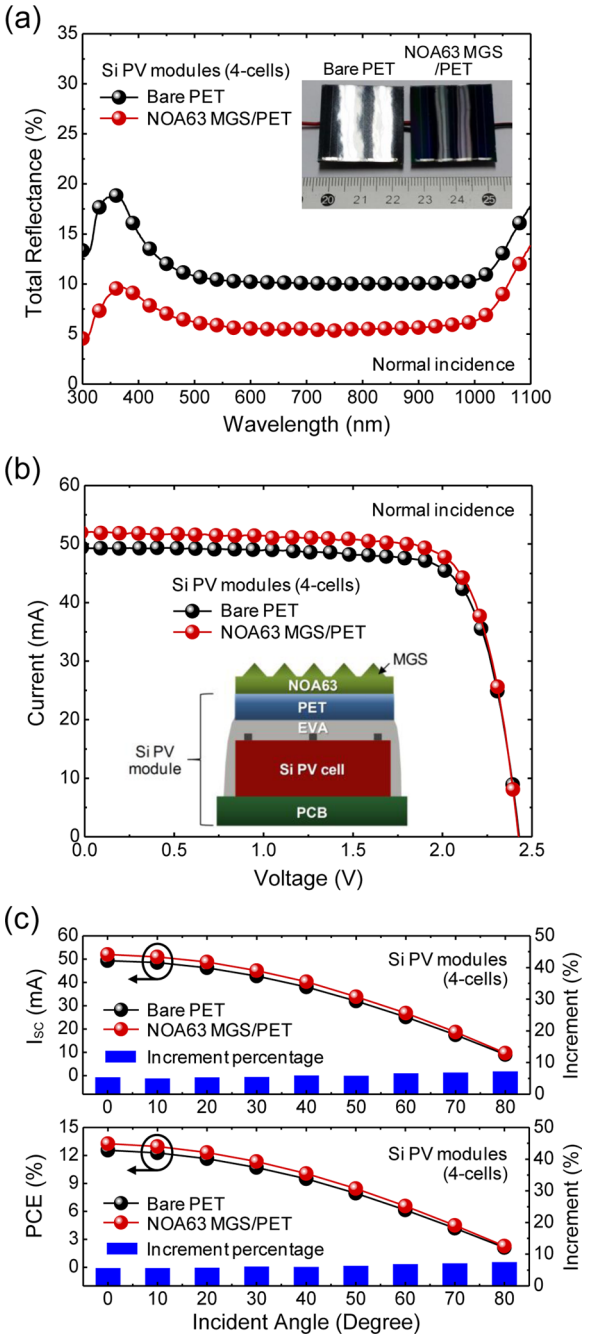

Figure 6. (a) Measured total reflectance spectra and (b) current−voltage (I−V) characteristics of Si PV modules (four cells) with the bare PET and NOA63 MGS/PET at normal incidence. (c) Measured I_{SC} and PCE of the Si PV modules with the bare PET and NOA63 MGS/PET as a function of light incident angle and the increment percentage in I_{SC} and PCE for the Si PV module with the NOA63 MGS relative to the reference Si PV module with the bare PET. Photograph of the corresponding assembled Si PV modules for I−V measurements for AR properties and schematic of Si PV modules with the NOA63 MGS/PET are also shown in the insets of (a) and (b), respectively.

shows the corresponding assembled Si PV modules for I−V measurements. In the photograph of Figure 6a, the white fluorescent light is strongly reflected at the surface of the reference Si PV module with the bare PET. In contrast, the Si PV module with the NOA63 MGS/PET exhibits a weak reflected white fluorescent light because of its low reflection

DOI: 10.1021/am5068194
ACS Appl. Mater. Interfaces 2015, 7, 2349−2358

Table 1. Measured $I-V$ Characteristics of Si PV Modules with Bare PET and NOA63 MGS/PET

Si PV module (4-cells)	V_{MAX} (V)	I_{MAX} (mA)	P_{MAX} (mW)	V_{OC} (V)	I_{SC} (mA)	FF (%)	PCE (%)
Bare PET	2.035	45.00	91.56	2.428	49.35	76.35	12.55
NOA63 MGS/PET	2.035	47.49	96.63	2.427	52.01	76.58	13.26

properties at visible wavelengths, as shown in the reflectance spectra of Figure 6a. The measured $I-V$ characteristics of Si PV modules with the bare PET and NOA63 MGS/PET are summarized in Table 1. From $I-V$ curves of Figure 6b, by incorporating the NOA63 MGS into the Si PV module, the short circuit current (I_{SC}) is improved from 49.35 to 52.01 mA, while there is no considerable variation for both the open circuit voltage (V_{OC}) and the fill factor (FF), exhibiting the I_{SC} increment percentage of ~5.4%. This I_{SC} increment percentage is similar or superior as compared to the results in PV cells or modules with various AR structured cover-substrates (i.e., I_{SC} increment percentage of ~2.2% for the WO_3-TiO_2 nanoparticle photocatalyst-coated coverglass,[5] ~2.4% for the AR moth-eye patterned polymer film/coverglass,[34] ~7% for the moth-eye patterned SiO_2 film/coverglass,[66] ~3.2% for the porous SiO_2 AR-coated coverglass[67] in Si-based PV modules, ~4.7% for the moth-eye structured coverglass in InGaP/GaAs/Ge triple-junction PV modules,[68] ~2.1% for the AR film-coated indium tin oxide-polyethylene naphthalate (ITO-PEN) film in encapsulated dye-sensitized solar cells,[69] ~2.9% for the nanostructured PET cover-substrate in encapsulated PV cells,[70] and ~2.7% for the moth-eye structured PMMA/coverglass in encapsulated organic PV cells[40]) reported in other previously published literatures. In these PV systems, the photocurrent improvement was also mainly caused by the enhanced transmission (i.e., ~2−3.8%) or suppressed reflection (i.e., ~3−3.5%) as compared to transparent cover-substrates with a bare surface due to the corresponding AR structures.[5,34,40,66−70] As a result, its PCE is enhanced by 13.26% (cf., PCE = 12.55% for the reference PV module with the bare PET), showing the PCE increment percentage of ~5.7%. This PCE increment percentage also exhibits a similar or higher value as compared to the results reported in other works.[5,34,40,66−70] However, to produce nanostructured transparent cover-substrates, expensive and complicated fabrication processes might be required.[23−31] Moreover, the polymers such as PDMS, PMMA, PC, and PU have a strong absorption in the NIR wavelength range of 800−1100 nm.[43−45] This PCE improvement is ascribed to the increased light absorption in the absorption layer of Si PV cells due to light harvesting effects of the NOA63 MGS polymer film including efficient AR and strong light scattering properties, as mentioned above.

The incident angle of solar irradiance is wide due to the diffused light scattered by the atmosphere and the positional variation of the sun in a day and the seasons. Thus, the light incident angle-dependent performance of PV modules is also important. Figure 6c shows the measured I_{SC} and PCE of Si PV modules with the bare PET and NOA63 MGS/PET as a function of light incident angle and the increment percentage in I_{SC} and PCE for the Si PV module with the NOA63 MGS relative to the reference Si PV module with the bare PET. As shown in Figure 6c, for $I-V$ measurements at different light incident angles, inclined mounts with tilting angles (θ_i) of 10−80° were used. As the θ_i value is increased, the I_{SC} values of both PV modules are dramatically decreased. This is mainly attributed to the reduction of the projection area where the incident light enters into the PV module due to the tilted PV module from the normally incident light source of the solar simulator, together with the increased surface reflection losses. Also, as can be seen in Figure S6 (Supporting Information), the V_{OC} values are slightly reduced due to the decreased I_{SC}, which can be found by the following equation:[14]

$$V_{OC} = \frac{E_g}{q} + \frac{nkT}{q}\ln(I_{SC}) - \frac{nkT}{q}\ln(I_0) \quad (4)$$

where E_g is the energy bandgap, n is the ideality factor, kT/q is the thermal voltage, and I_0 is the saturation current, related to the material quality. Meanwhile, the FF is kept at similar values. As a result, the PCE of the Si PV module is gradually degraded with increasing θ_i value. However, for the PCE, the Si PV module with the NOA63 MGS/PET exhibits a superior solar power generation as compared to the reference PV module with the bare PET over a wide θ_i range of 10−80°. The corresponding increment percentage values of the Si PV module with the NOA63 MGS/PET against one with the bare PET in both the I_{SC} and the PCE are higher than 5% at each θ_i value, exhibiting the average increment percentage values of ~6% for the I_{SC} and ~6.3% for the PCE for θ_i = 10−80°. From these results, for Si-based PV modules covered by PET protection films, the use of the NOA63 MGS polymer films with efficient light harvesting can further boost the solar energy conversion efficiency for the entire day and season without a costly solar tracking system.

4. CONCLUSION

The solar power generation enhancement of Si PV modules with the conical MG patterned NOA63 polymer films for an efficient light harvesting and protection, fabricated by the soft imprint lithography, on PET cover-substrates was reported. The black charcoal dusts on NOA63 MGS polymer films with a hydrophobic surface (i.e., $\theta_{CA} \approx 121°$ at no inclination and $\theta_{ACA}/\theta_{RCA} \approx 132°/111°$ at the inclination angle of 40°) were well removed by rolling-down water droplets. More importantly, the structure led to the considerable improvement of the total and diffuse transmittances of the bare PET, simultaneously, over a wide wavelength range of 300−1100 nm, exhibiting higher $T_{SW} \approx 93.1\%$ and $H_{Avg} \approx 88.3\%$ as well as lower $R_{SW} \approx 8.2\%$ than those (i.e., $T_{SW} \approx 86.9\%$, $H_{Avg} \approx 9.1\%$, $R_{SW} \approx 13.5\%$) of the bare PET. The light scattering effect of NOA63 MGS was theoretically studied by the FDTD calculation. Also, it showed relatively good transmittance properties after heat treatments, exhibiting the T_{SW} value of ~91.6% at the high temperature of 160 °C. By employing the NOA63 MGS polymer layer into the surface of the PET cover-substrate in Si PV modules as a light harvesting and protection film, the improved I_{SC} and PCE values were obtained as compared to the reference PV module with the bare PET in a wide θ_i range of 0−80°, showing the average increment percentage value of ~6.3% in the PCE. Additionally, it is noticeable that the NOA63 polymer films with conical MG pattern arrays can be applied to other PV systems as well as various optical/optoelectronic devices that use transparent substrates and covers including glasses, plastics, polymers, and

DOI: 10.1021/am5068194
ACS Appl. Mater. Interfaces 2015, 7, 2349−2358

quartzes. These results can provide a promising potential of multifunctional NOA63 MGS polymer films, which can be easily prepared by simple and inexpensive soft imprint lithography, including efficient omnidirectional broadband light harvesting (i.e., AR and light scattering properties), high-tolerance, and self-cleaning for high-performance PV system applications.

■ ASSOCIATED CONTENT

Supporting Information

SEM and photograph images of NOA63 MGS/PET, wetting behavior of the flat NOA63 film/PET and dynamic wetting behavior of the NOA63 MGS/PET, sequential photographs of water droplet cleaning behaviors of the NOA63 MGS/PET, measured total/diffuse transmittance and total reflectance spectra of the flat NOA63 film/PET, and V_{OC} and FF of Si PV modules with the bare PET and NOA63 MGS/PET as a function of light incident angle. This material is available free of charge via the Internet at http://pubs.acs.org.

■ AUTHOR INFORMATION

Corresponding Author

*Tel.: +82-31-201-3820. Fax: +82-31-206-2820. E-mail: jsyu@khu.ac.kr.

Notes

The authors declare no competing financial interest.

■ ACKNOWLEDGMENTS

This work was supported by the National Research Foundation of Korea (NRF) grant funded by the Korea government (MSIP) (no. 2013-068407).

■ REFERENCES

(1) Battaglia, C.; Escarré, J.; Söderström, K.; Charriére, M.; Despeisse, M.; Haug, F. J.; Ballif, C. Nanomoulding of Transparent Zinc Oxide Electrodes for Efficient Light Trapping in Solar Cells. *Nat. Photonics* **2011**, *5*, 535−538.

(2) Leem, J. W.; Jun, D. H.; Heo, J.; Park, W. K.; Park, J. H.; Cho, W. J.; Kim, D. E.; Yu, J. S. Single-Material Zinc Sulfide Bi-Layer Antireflection Coatings for GaAs Solar Cells. *Opt. Express* **2013**, *21*, A821−A828.

(3) Kim, S.; Koh, J. H.; Yang, X.; Chi, W. S.; Park, C.; Leem, J. W.; Kim, B.; Seo, S.; Kim, Y.; Yu, J. S.; Kim, J. H.; Kim, E. Enhanced Device Efficiency of Bilayered Inverted Organic Solar Cells Based on Photocurable P3HTs with a Light-Harvesting ZnO Nanorod Array. *Adv. Energy Mater.* **2014**, *4*, 1301338.

(4) Jiang, W. T.; Wu, C. T.; Sung, Y. H.; Wu, J. J. Room-Temperature Fast Construction of Outperformed ZnO Nanoarchitectures on Nanowire-Array Templates for Dye-Sensitized Solar Cells. *ACS Appl. Mater. Interfaces* **2013**, *5*, 911−917.

(5) Noh, H. N.; Myong, S. Y. Antireflective Coating Using a WO_3-TiO_2 Nanoparticle Photocatalytic Composition for High Efficiency Thin-Film Si Photovoltaic Modules. *Sol. Energy Mater. Sol. Cells* **2014**, *121*, 108−113.

(6) Shah, A.; Meier, J.; Buechel, A.; Kroll, U.; Steinhauser, J.; Meillaud, F.; Schade, H.; Dominé, D. Towards Very Low-Cost Mass Production of Thin-Film Silicon Photovoltaic (PV) Solar Modules on Glass. *Thin Solid Films* **2006**, *502*, 292−299.

(7) Metz, A.; Adler, D.; Bagus, S.; Blanke, H.; Bothar, M.; Brouwer, E.; Dauwe, S.; Dressler, K.; Droessler, R.; Droste, T.; Fiedler, M.; Gassenbauer, Y.; Grahl, T.; Hermert, N.; Kuzminsk, W.; Lachowicz, A.; Lauinger, T.; Lenck, N.; Manole, M.; Martini, M.; Messmer, R.; Meyer, C.; Moschner, J.; Ramspeck, K.; Roth, P.; Schönfelder, R.; Schum, B.; Sticksel, J.; Vaas, K.; Volk, M.; Wangemann, K. Industrial High Performance Crystalline Silicon Solar Cells and Modules Based on Rear Surface Passivation Technology. *Sol. Energy Mater. Sol. Cells* **2014**, *120*, 417−425.

(8) Yang, S. M.; Hsieh, Y. C.; Jeng, C. A. Optimal Design of Antireflection Coating and Experimental Verification by Plasma Enhanced Chemical Vapor Deposition in Small Displays. *J. Vac. Sci. Technol., A* **2009**, *27*, 336−341.

(9) Kadakia, N.; Naczas, S.; Bakhru, H.; Huang, M. Fabrication of Surface Textures by Ion Implantation for Antireflection of Silicon Crystals. *Appl. Phys. Lett.* **2010**, *97*, 191912.

(10) Leem, J. W.; Song, Y. M.; Yu, J. S. Broadband Antireflective Germanium Surfaces Based on Subwavelength Structures for Photovoltaic Cell Applications. *Opt. Express* **2011**, *19*, 26308−26317.

(11) Song, Y. M.; Jang, S. J.; Yu, J. S.; Lee, Y. T. Bioinspired Parabola Subwavelength Structures for Improved Broadband Antireflection. *Small* **2010**, *6*, 984−987.

(12) Leem, J. W.; Yu, J. S.; Heo, J.; Park, W. K.; Park, J. H.; Cho, W. J.; Kim, D. E. Nanostructured Encapsulation Coverglasses with Wide-Angle Broadband Antireflection and Self-Cleaning Properties for III-V Multi-Junction Solar Cell Applications. *Sol. Energy Mater. Sol. Cells* **2014**, *120*, 555−560.

(13) Leem, J. W.; Chung, K. S.; Yu, J. S. Antireflective Properties of Disordered Si SWSs with Hydrophobic Surface by Thermally Dewetted Pt Nanomask Patterns for Si-Based Solar Cells. *Curr. Appl. Phys.* **2012**, *12*, 291−298.

(14) Yeh, L. K.; Lai, K. Y.; Lin, G. J.; Fu, P. H.; Chang, H. C.; Lin, C. A.; He, J. H. Giant Efficiency Enhancement of GaAs Solar Cells with Graded Antireflection Layers Based on Syringelike ZnO Nanorod Arrays. *Adv. Energy Mater.* **2011**, *1*, 506−510.

(15) Ji, S.; Song, K.; Nguyen, T. B.; Kim, N.; Lim, H. Optimal Moth Eye Nanostructure Array on Transparent Glass Towards Broadband Antireflection. *ACS Appl. Mater. Interfaces* **2013**, *5*, 10731−10737.

(16) Leem, J. W.; Song, Y. M.; Yu, J. S. Biomimetic Artificial Si Compound Eye Surface Structures with Broadband and Wide-Angle Antireflection Properties for Si-Based Optoelectronic Applications. *Nanoscale* **2013**, *5*, 10455−10460.

(17) Ko, Y. H.; Yu, J. S. Highly Transparent Sapphire Micro-Grating Structures with Large Diffuse Light Scattering. *Opt. Express* **2011**, *19*, 15574−15583.

(18) Cheng, Y. T.; Ho, J. J.; Tsai, S. Y.; Ye, Z. Z.; Lee, W.; Hwang, D. S.; Chang, S. H.; Chang, C. C.; Wang, K. L. Efficiency Improved by Acid Texturization for Multi-Crystalline Silicon Solar Cells. *Sol. Energy* **2011**, *85*, 87−94.

(19) Chen, Y. P.; Lee, C. H.; Wang, L. A. Fabrication and Characterization of Multi-Scale Microlens Arrays with Anti-Reflection and Diffusion Properties. *Nanotechnology* **2011**, *22*, 215303.

(20) Ho, C. H.; Lien, D. H.; Chang, H. C.; Lin, C. A.; Kang, C. F.; Hsing, M. K.; Lai, K. Y.; He, J. H. Hierarchical Structures Consisting of SiO_2 Nanorods and p-GaN Microdomes for Efficiently Harvesting Solar Energy for InGaN Quantum Well Photovoltaic Cells. *Nanoscale* **2012**, *4*, 7346−7349.

(21) Song, Y. M.; Xie, Y.; Malyarchuk, V.; Xiao, J.; Jung, I.; Choi, K. J.; Liu, Z.; Park, H.; Lu, C.; Kim, R. H.; Li, R.; Crozier, K. B.; Huang, Y.; Rogers, J. A. Digital Cameras with Designs Inspired by the Arthropod Eye. *Nature* **2013**, *497*, 95−99.

(22) Tsui, K. H.; Lin, Q.; Chou, H.; Zhang, Q.; Fu, H.; Qi, P.; Fan, Z. Low-Cost, Flexible, and Self-Cleaning 3D Nanocone Anti-Reflection Films for High-Efficiency Photovoltaics. *Adv. Mater.* **2014**, *26*, 2805−2811.

(23) Toyota, H.; Takahara, K.; Okano, M.; Yotsuya, T.; Kikuta, H. Fabrication of Microcone Array for Antireflection Structured Surface Using Metal Dotted Pattern. *Jpn. J. Appl. Phys.* **2001**, *40*, L747−L749.

(24) Asadollahbaik, A.; Boden, S. A.; Charlton, M. D. B.; Payne, D. N. R.; Cox, S.; Bagnall, D. M. Reflectance Properties of Silicon Moth-Eyes in Response to Variations in Angle of Incidence. Polarisation and Azimuth Orientation. *Opt. Express* **2014**, *22*, A402−A415.

(25) Yu, Z.; Gao, H.; Wu, W.; Ge, H.; Chou, S. Y. Fabrication of Large Area Subwavelength Antireflection Structures on Si Using Trilayer Resist Nanoimprint Lithography and Liftoff. *J. Vac. Sci. Technol., B* **2003**, *21*, 2874−2877.

DOI: 10.1021/am5068194
ACS Appl. Mater. Interfaces 2015, 7, 2349−2358

(26) Chen, K.; Azhar, E.; Ma, T.; Jiang, H.; Yu, H. Facile Large-Area Photolithography of Periodic Sub-Micron Structures Using a Self-Formed Polymer Mask. *Appl. Phys. Lett.* **2012**, *100*, 233503.
(27) Luo, Y.; Misra, V. Large-Area Long-Range Ordered Anisotropic Magnetic Nanostructure Fabrication by Photolithography. *Nanotechnology* **2006**, *17*, 4909−4911.
(28) Ji, S.; Park, J.; Lim, H. Improved Antireflection Properties of Moth Eye Mimicking Nanopillars on Transparent Glass: Flat Antireflection and Color Tuning. *Nanoscale* **2012**, *4*, 4603−4610.
(29) Phillips, B. M.; Jiang, P.; Jiang, B. Biomimetic Broadband Antireflection Gratings on Solar-Grade Multicrystalline Silicon Wafers. *Appl. Phys. Lett.* **2011**, *99*, 191103.
(30) Leem, J. W.; Yu, J. S. Wafer-Scale Highly-Transparent and Superhydrophilic Sapphires for High-Performance Optics. *Opt. Express* **2012**, *20*, 26160−26166.
(31) Leem, J. W.; Yu, J. S.; Jun, D. H.; Heo, J.; Park, W. K. Efficiency Improvement of III-V GaAs Solar Cells Using Biomimetic TiO_2 Subwavelength Structures with Wide-Angle and Broadband Antireflection Properties. *Sol. Energy Mater. Sol. Cells* **2014**, *127*, 43−49.
(32) Ahn, S. H.; Guo, L. J. Large-Area Roll-to-Roll and Roll-to-Plate Nanoimprint Lithography: A Step Toward High-Throughput Application of Continuous Nanoimprinting. *ACS Nano* **2009**, *3*, 2304−2310.
(33) Krebs, F. C. Polymer Solar Cell Modules Prepared Using Roll-to-Roll Methods: Knife-over-Edge Coating, Slot-Die Coating and Screen Printing. *Sol. Energy Mater. Sol. Cells* **2009**, *93*, 465−475.
(34) Lee, S. H.; Han, K. S.; Shin, J. H.; Hwang, S. Y.; Lee, H. Fabrication of Highly Transparent Self-Cleaning Protection Films for Photovoltaic Systems. *Prog. Photovoltaics* **2013**, *21*, 1056−1062.
(35) Su, H.; Zhang, M.; Chang, Y. H.; Zhai, P.; Hau, N. Y.; Huang, Y. T.; Liu, C.; Soh, A. K.; Feng, S. P. Highly Conductive and Low Cost Ni-PET Flexible Substrate for Efficient Dye-Sensitized Solar Cells. *ACS Appl. Mater. Interfaces* **2014**, *6*, 5577−5584.
(36) Espinosa, N.; García-Valverde, R.; Krebs, F. C. Life-Cycle Analysis of Product Integrated Polymer Solar Cells. *Energy Environ. Sci.* **2011**, *4*, 1547−1557.
(37) Filmetrics Refractive Index Database, retrieved 2014, http://www.filmetrics.com/refractive-index-database.
(38) Leem, J. W.; Kim, S.; Lee, S. H.; Rogers, J. A.; Kim, E.; Yu, J. S. Efficiency Enhancement of Organic Solar Cells Using Hydrophobic Antireflective Inverted Moth-Eye Nanopatterned PDMS Films. *Adv. Energy Mater.* **2014**, *4*, 1301315.
(39) Galeotti, F.; Trespidi, F.; Timò, G.; Pasini, M. Broadband and Crack-Free Antireflection Coatings by Self-Assembled Moth Eye Patterns. *ACS Appl. Mater. Interfaces* **2014**, *6*, 5827−5834.
(40) Forbeich, K.; Dennler, G.; Scharber, M. C.; Hingerl, K.; Fromherz, T.; Brabec, C. J. Performance Improvement of Organic Solar Cells with Moth Eye Anti-Reflection Coating. *Thin Solid Films* **2008**, *516*, 7167−7170.
(41) Kanamori, Y.; Hane, K. Broadband Antireflection Subwavelength Gratings for Polymethyl Methacrylate Fabricated with Molding Technique. *Opt. Rev.* **2002**, *9*, 183−185.
(42) Ko, D. H.; Tumbleston, J. R.; Henderson, K. J.; Euliss, L. E.; Desimone, J. M.; Lopez, R.; Samulski, E. T. Biomimetic Microlens Array with Antireflective "Moth-Eye" Surface. *Soft Mater.* **2011**, *7*, 6404−6407.
(43) Cai, D. K.; Neyer, A.; Kuckuk, R.; Heise, H. M. Optical Absorption in Transparent PDMS Materials Applied for Multimode Waveguides Fabrication. *Opt. Mater.* **2008**, *30*, 1157−1161.
(44) Kim, D. S.; Jeong, Y.; Jeong, H.; Jang, J. H. Triple-Junction InGap/GaAs/Ge Solar Cells Integrated with Polymethyl Metacrylate Subwavelength Structure. *Appl. Surf. Sci.* **2014**, *320*, 901−907.
(45) Aden, M.; Roesner, A.; Olowinsky, A. Optical Characterization of Polycarbonate: Influence of Additives on Optical Properties. *J. Polym. Sci., Part B: Polym. Phys.* **2010**, *48*, 451−455.
(46) Norland Optical Adhesive, retrieved 2014, https://www.norlandprod.com.
(47) Myers, J. D.; Cao, W.; Cassidy, V.; Eom, S. H.; Zhou, R.; Yang, L.; You, W.; Xue, J. A Universal Optical Approach to Enhancing Efficiency of Organic-Based Photovoltaic Devices. *Energy Environ. Sci.* **2012**, *5*, 6900−6904.
(48) Heo, S. Y.; Koh, J. K.; Kang, G.; Ahn, S. H.; Chi, W. S.; Kim, K.; Kim, J. H. Bifunctional Moth-Eye Nanopatterned Dye-Sensitized Solar Cells: Light-Harvesting and Self-Cleaning Effects. *Adv. Energy Mater.* **2014**, *4*, 1300632.
(49) Lee, M. J.; Lee, N. Y.; Lim, J. R.; Kim, J. B.; Kim, M.; Baik, H. K.; Kim, Y. S. Antiadhesion Surface Treatments of Molds for High-Resolution Unconventional Lithography. *Adv. Mater.* **2006**, *18*, 3115−3119.
(50) Kim, Y. S.; Lee, N. Y.; Lim, J. R.; Lee, M. J.; Park, S. Nanofeature-Patterned Polymer Mold Fabrication Toward Precisely Defined Nanostructure Replication. *Chem. Mater.* **2005**, *17*, 5867−5870.
(51) Choi, Y. W.; Han, J. E.; Lee, S.; Sohn, D. Preparation of a Superhydrophobic Film with UV Imprinting Technology. *Macromol. Res.* **2009**, *17*, 821−824.
(52) Park, Y. B.; Im, H.; Im, M.; Choi, Y. K. Self-Cleaning Effect of Highly Water-Repellent Microshell Structures for Solar Cell Applications. *J. Mater. Chem.* **2011**, *21*, 633−636.
(53) Zhu, J.; Hsu, C. M.; Yu, Z.; Fan, S.; Cui, Y. Nanodome Solar Cells with Efficient Light Management and Self-Cleaning. *Nano Lett.* **2010**, *10*, 1979−1984.
(54) Cassie, A. B. D.; Baxter, S. Wettability of Porous Surfaces. *Trans. Faraday Soc.* **1944**, *40*, 546−551.
(55) Ranella, A.; Barberoglou, M.; Bakogianni, S.; Fotakis, C.; Stratakis, E. Tuning Cell Adhesion by Controlling the Roughness and Wettability of 3D Micro/Nano Silicon Structures. *Acta Biomater.* **2010**, *6*, 2711−2720.
(56) Hong, D.; Ryu, I.; Kwon, H.; Lee, J. J.; Yim, S. Preparation of Superhydrophobic, Long-Neck Vase-Like Polymer Surfaces. *Phys. Chem. Chem. Phys.* **2013**, *15*, 11862−11867.
(57) Xi, J. Q.; Schubert, M. F.; Kim, J. K.; Schubert, E. F.; Chen, M.; Lin, S. Y.; Liu, W.; Smart, J. A. Optical Thin-Film Materials with Low Refractive Index for Broadband Elimination of Fresnel Reflection. *Nat. Photonics* **2007**, *1*, 176−179.
(58) Woo, S. H.; Park, Y. J.; Chang, D. H.; Sobahan, K. M. A.; Hwangbo, C. K. Wideband Antireflection Coatings of Porous MgF_2 Films by Using Glancing Angle Deposition. *J. Korean Phys. Soc.* **2007**, *51*, 1501−1506.
(59) Leem, J. W.; Song, Y. M.; Yu, J. S. Broadband Wide-Angle Antireflection Enhancement in AZO/Si Shell/Core Subwavelength Grating Structures with Hydrophobic Surface for Si-Based Solar Cells. *Opt. Express* **2011**, *19*, A1155−A1164.
(60) NREL's Renewable Resource Data Center, retrieved 2014, http://rredc.nrel.gov/solar/spectra/am1.5.
(61) Cui, H.; Pillai, S.; Campbell, P.; Green, M. A Novel Silver Nanoparticle Assisted Texture as Broadband Antireflection Coating for Solar Cell Applications. *Sol. Energy Mater. Sol. Cells* **2013**, *109*, 233−239.
(62) Zhao, J.; Green, M. A. Optimized Antireflection Coatings for High-Efficiency Silicon Solar Cells. *IEEE Trans. Electron Devices* **1991**, *38*, 1925−1934.
(63) Boden, S. A.; Bagnall, D. M. Sunrise to Sunset Optimization of Thin Film Antireflective Coatings for Encapsulated, Planar Silicon Solar Cells. *Prog. Photovoltaics* **2009**, *17*, 241−252.
(64) Martel, A.; Caballero-Briones, F.; Castro-Rodríguez, R.; Méndez-Gamboa, J.; Rromeo, N.; Bosio, A.; Peña, J. L. Physical Properties of Transparent Conducting Cd-Te-In-O Thin Films Outlining a Thermodynamic System for Transparent Conducting Oxides. *Thin Solid Films* **2009**, *518*, 413−418.
(65) Hecht, E. *Optics*, 4th ed.; Addison Wesley: San Francisco, CA, 2002.
(66) Shin, J. H.; Kim, Y. D.; Choi, H. J.; Ryu, S. W.; Lee, H. Multi-Functional SiO_2 Moth-Eye Pattern for Photovoltaic Applications. *Sol. Energy Mater. Sol. Cells* **2014**, *126*, 1−5.
(67) Raut, H. K.; Nair, A. S.; Dinachali, S. S.; Ganesh, V. A.; Walsh, T. M.; Ramakrishna, S. Porous SiO_2 Anti-Reflective Coatings on

DOI: 10.1021/am5068194
ACS Appl. Mater. Interfaces 2015, 7, 2349−2358

Large-Area Substrates by Electrospinning and Their Application to Solar Modules. *Sol. Energy Mater. Sol. Cells* **2013**, *111*, 9−15.
(68) Song, Y. M.; Jeong, Y.; Yeo, C. I.; Lee, Y. T. Enhanced Power Generation in Concentrated Photovoltaics Using Broadband Antireflective Coverglasses with Moth Eye Structures. *Opt. Express* **2012**, *20*, A916−A923.
(69) Yamaguchi, T.; Tobe, N.; Matsumoto, D.; Nagai, T.; Arakawa, H. Highly Efficient Plastic-Substrate Dye-Sensitized Solar Cells with Validated Conversion Efficiency of 7.6%. *Sol. Energy Mater. Sol. Cells* **2010**, *94*, 812−816.
(70) Liu, S. J.; Liao, C. T. Fast Fabrication of Nano-Structured Antireflection Layers for Enhancement of Solar Cells Performance Using Plasma Sputtering and Infrared Assisted Roller Embossing Techniques. *Opt. Express* **2012**, *20*, 5143−5150.

DOI: 10.1021/am5068194
ACS Appl. Mater. Interfaces 2015, 7, 2349−2358